NIST's New 3D Airspeed Calibration Rig Addresses Turbulent Flow Measurement Challenges

Iosif I. Shinder, Vladimir B. Khromchenko, Michael R. Moldover

Flow Metrology Group, Sensor Science Division
National Institute of Standards and Technology, Gaithersburg, MD, 20899-8360 USA
Corresponding Author: Iosif.Shinder@nist.gov

Abstract

Outdoor air flows and flue-gas flows in large conduits and large stacks have significant swirl and turbulence. Accurate measurements of such complex flows are needed by weather services and diverse industries (*e.g.* automotive, aircraft, wind-power, fossil-fueled electricity-generating). The instruments used for accurately measuring complex flows must be calibrated under conditions similar to the conditions encountered when these instruments are used in the field. To meet this requirement, NIST developed a 3-dimensional (3-D) calibration rig that orients test instruments at user-selected pitch angles (−45 ° to 45 °) and yaw angles (-180 ° to +180 °) with a resolution of 0.1 ° with respect to the air flow in NIST's wind tunnel. The rig accommodates probes up to 2.5 m long and achieves an expanded air speed uncertainty of approximately 1% (95 % confidence level) over the range 5 m/s to 45 m/s. For measurements in turbulence intensities up to 20 %, we install turbulence-generating flow conditioners in the wind tunnel. We tested four methods of measuring turbulence intensity: (1), laser doppler anemometer, (2) high-frequency, 3-D multi-hole, pressure probe, (3) constant-temperature hot-wire anemometer, and (4) L-shaped pitot tube. Methods (1), (2), and (3) were in mutual agreement. This agreement implies that NIST's new rig can measure the response of virtually any anemometer or probe to a well-defined airspeed vector at diverse turbulence levels. The data from the L-shaped pitot tube [Method (4)] must be corrected for the response time of the differential pressure gauge and for flow in the tubes connecting the pitot tube to the pressure gauge. We illustrate NIST's new capabilities by displaying turbulence-dependent calibrations of an L-shaped pitot tube, a conical pressure probe (mutli-hole, 3-D pitot tube), and an S-probe (a two-port pressure probe that is widely used to measure flue gas flows in the stacks of power plants).

1. Introduction

This manuscript describes the evolution of the National Institute of Standards and Technology (NIST) airspeed calibration facility toward increasing versatility and increasing relevance to the metrology of turbulent flows. The starting point is NIST's low-turbulence (≈ 0.1 %) wind tunnel which has been used for 40 years to calibrate air-flow meters under test (MUT) as a function of manually-selected air speeds at a single orientation with respect to the flow. [1] Today, the facility can calibrate the MUT using multiple, computer-selected, air speeds and multiple computer-selected orientations. At present, we use manually-installed, passive, turbulence generators to generate and measure turbulence intensities from 0.1 % to

20 % at the MUT. Ultimately, we hope to install an active turbulence generator that operates under computer control. This will enable NIST to routinely calibrate MUTs in turbulent flows.

Traditionally, NIST has conducted airspeed calibrations in its closed, low-turbulence wind tunnel. [2] To conform to calibration conventions and to precisely define the orientation of the MUT with respect to the air flow, NIST minimizes the turbulence and fan-generated swirl in the test volume. Turbulence and swirl are reduced in a large-cross-section "settling" chamber upstream of the test volume. The settling chamber contains flow-conditioning devices and it is joined to the test volume by a smooth, contracting connection. To achieve the smallest-practical calibration uncertainties, the test volume of NIST's wind tunnel has a large cross section (2.1 m × 1.5 m) that minimizes the disturbances of the air flow from the tunnel's walls and from blockage of the flow by the MUT. Similar to NIST, the National Metrology Institutes of other countries conduct airspeed calibrations in large, low-turbulence wind tunnels. [3]

Outdoor air flows and flue-gas flows in large stacks always have spatial and temporal non-uniformities; such flows are called "swirling", "eddying", and "turbulent". These non-uniformities change the responses of a MUT in complex ways that depend upon the physical principles underlying the operation of the MUT as well as the MUT's size, orientation, frequency response, electronics, *etc.* In certain ideal cases, the responses are predictable; for example, homogeneous turbulence is predicted to change the calibration of pitot tubes in proportion to the square of the turbulence intensity. In other cases, the responses are too complex to predict quantitatively. For example, the separation of the boundary layer from a multi-hole pressure probe causes its calibration factor to have hysteresis of up to 15 % on increasing and decreasing flows for particular orientations and air speeds. [4] This is shown in Fig 10, below.

We used an L-shaped pitot tube and an S-probe as MUTs during our first calibrations in turbulent flows. These rugged sensors are important because they are widely used to conduct relative accuracy test audits (RATA) calibrations of continuous emission monitoring systems (CEMS). (Because the RATA tests are *relative*, they are not traceable to the International System of Units, the SI.) CEMS systems are installed in the flue-gas stacks of coal-burning power plants to comply with local, state, and federal emissions regulations. We anticipate that carbon controls (such as a carbon tax or cap-and-trade market) will require accurate CO_2 flux measurements that are traceable to the international system of units to provide the technical basis for enforcing carbon controls. Thus, one goal of this research is characterize L-shaped pitot tubes and S-probes in complex flows such as those found in flue-gas stacks.

2. Generating Turbulence

In 1934, Simmons and Salter introduced the idea of generating turbulence by placing grids of various shapes across the flow in a wind tunnel. [5] In 1935, Taylor developed a theory of grid induced turbulence. [6] Grid-generated turbulence is nearly homogeneous turbulence without eddies larger than the elements of the grid (or mesh); therefore, the generated turbulence scales with the size of the grid. We used two different grids to generate turbulence. One grid was a metal screen with square holes (15 mm on a side) separated by 3 mm of metal. The second grid was an array of 25 mm diameter wooden rods arranged to form square openings 125 mm on a side. (See Fig. 1, left.) The wooden grid generated a maximum turbulence intensity of 15 % at approximately 60 cm downstream from the grid for flows in the range 5 m/s to 25 m/s. Smaller values of the turbulence intensity were developed further downstream

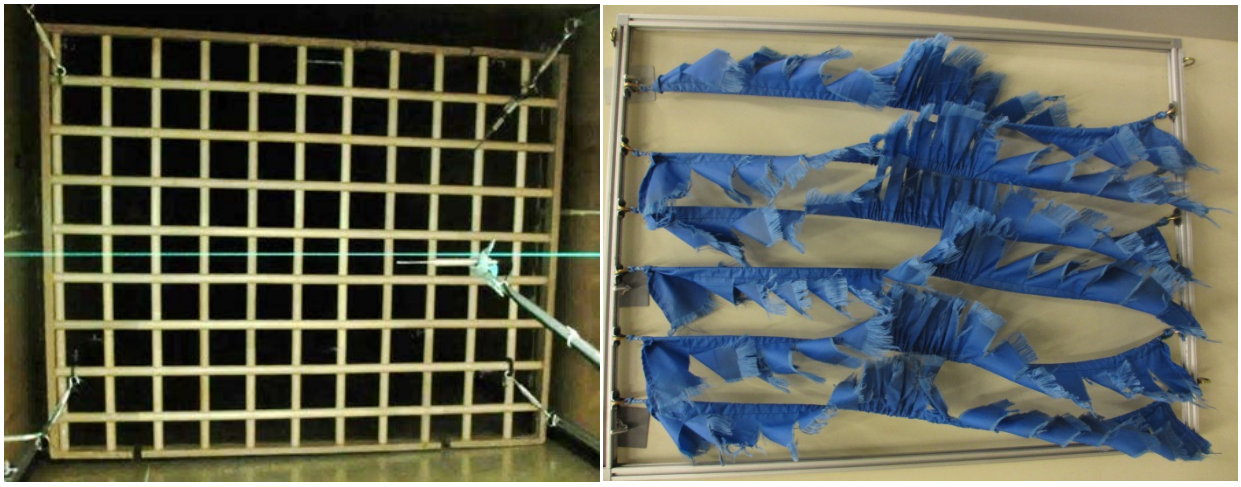

Figure 1. LEFT: Turbulence-generating wooden grid temporarily installed in NIST's wind tunnel. The wooden rods are 15 cm apart. An L-shaped pitot tube and the green light from the LDA are visible downstream from the grid. RIGHT: An array of turbulence-generating "flags" sewn onto ropes. Each rope is tied to a frame 1.25 m wide and 0.95 m high that can be installed in the wind tunnel.

from the grid. The spectrum of grid generated turbulence is discussed in [7]. For more information concerning turbulence from passive grids, see references [8,9].

To generate higher-intensity turbulence, we installed an array of "flags" into the wind tunnel. (See Fig. 1, right). Each flag was a nylon strip approximately 15 cm long and 8 cm wide. Each flag was sewn around a rope that was tied to a frame which could be easily installed and removed from the wind tunnel. At air speeds above 15 m/s, the flags began to fray. To stabilize the flags, we "trained" the assembled flag array for approximately 30 minutes at 25 m/s. After the training, turbulence intensity measured 50 cm downstream from the array was 20 % and stable in air speed ranging from 5 m/s to 35 m/s. At air speeds below 3 m/s, the flags moved only slightly and generated little turbulence. At airspeeds near 5 m/s, the flags generated a wide frequency spectrum with peaks near 5 Hz and its harmonics. (See Fig. 2.) At higher air speeds, the peaks in the turbulence spectrum moved to higher frequencies and became less prominent. The spectrum of turbulence generated by a single flag is discussed in [10, 11]. We are not aware of a publication describing the spectrum generated by an array of flags.

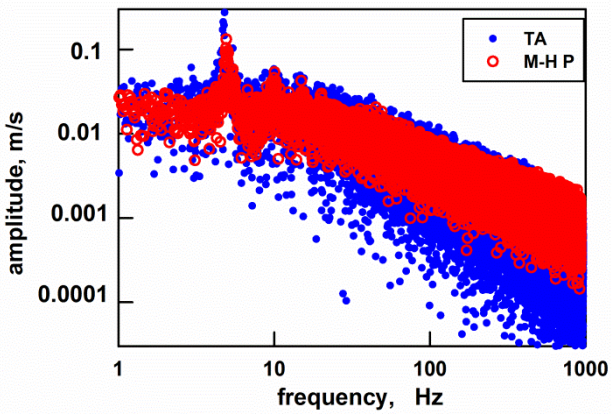

Figure 2. Spectrum of turbulence intensity generated by the flag array at 5 m/s. "TA" indicates measurements made with a hot-wire anemometer; "M-H P" indicates measurements made with a multi-hole pressure probe.

Larssen and Devenport developed an active grid that generated turbulence intensities up to 20 %. [12] Their generator was an array of rhombus-shaped vanes mounted on rods that were rotated by servo motors. They programmed the servo

motors to produce nearly-homogeneous turbulence with a flat mean velocity profile. We are considering the installation of such an active grid in NIST's wind tunnel..

3. Measuring turbulence intensity

We tested four methods of measuring turbulence intensity: (1) Laser Doppler anemometer (LDA), (2) high-frequency, 3-D, multi-hole pressure probe, (3), constant-temperature hot-wire, anemometer and (4) L-shaped pitot tube. As shown in Fig. 2, methods (1), (2), and (3) were in mutual agreement (within ±10 % for 95% confidence interval) for turbulence intensities from 2 % to 20 % and air speeds from 5 m/s to 25 m/s. In contrast, the turbulence intensities measured with the L-shaped pitot tube were only 19 % to 0.37 % of the intensities measured with the LDA. (See the dashed lines in Fig. 3.) We did not study the origin of this difference; we speculate that the higher-frequency pressure fluctuations at the pitot tube were attenuated by the response time of the differential pressure gauge and the time constant associated with flow in the tubes that connected the pitot tube to the pressure gauge.

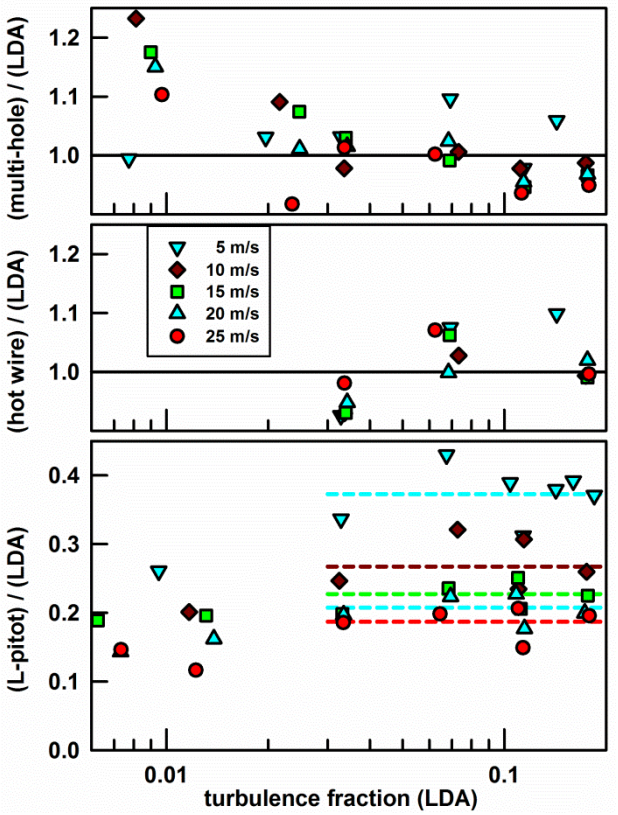

Figure 3. Turbulence intensities *Tu* measured with 4 instruments. The intensity ratios $Tu_{\text{multi-hole}}/Tu_{\text{LDA}}$ and $Tu_{\text{hot-wire}}/Tu_{\text{LDA}}$ are near 1.0, independent of air speed and turbulence fraction. The ratios $Tu_{\text{L-pitot}}/Tu_{\text{LDA}}$ range from 0.19 to 0.37 (dashed lines), depending on air speed.

3.1 Measuring turbulence with an LDA

For the comparisons shown in Fig. 2, we used the LDA as a working standard. The LDA was model FiberFlow model 60X11 manufactured by Dantec Dynamics[1]. For the LDA, we defined the turbulence intensity *Tu* by

$$Tu = \frac{\sigma_u}{\langle V \rangle} = \sqrt{\sigma_{Tu}^2 - \sigma_{BG}^2} \quad , \qquad (1)$$

where σ_μ is the standard deviation of the component of the velocity measured by the LDA, $\langle V \rangle$ is mean air speed measured by the LDA, σ_{Tu} is standard deviation of the LDA signal and σ_{BG} is the standard deviation of the LDA signal in the absence of turbulence. Figure 4 shows typical data from the burst spectrum analyzer of the LDA taken in two separate runs with $\langle V \rangle \approx 9.7$ m/s, $Tu = 0.052$, and $\sigma_{BG}/\langle V \rangle =$

[1]In order to describe materials and procedures adequately, it is occasionally necessary to identify commercial products by manufacturer's name or label. In no instance does such identification imply endorsement by the National Institute of Standards and Technology, nor does it imply that the particular product or equipment is necessarily the best available for the purpose.

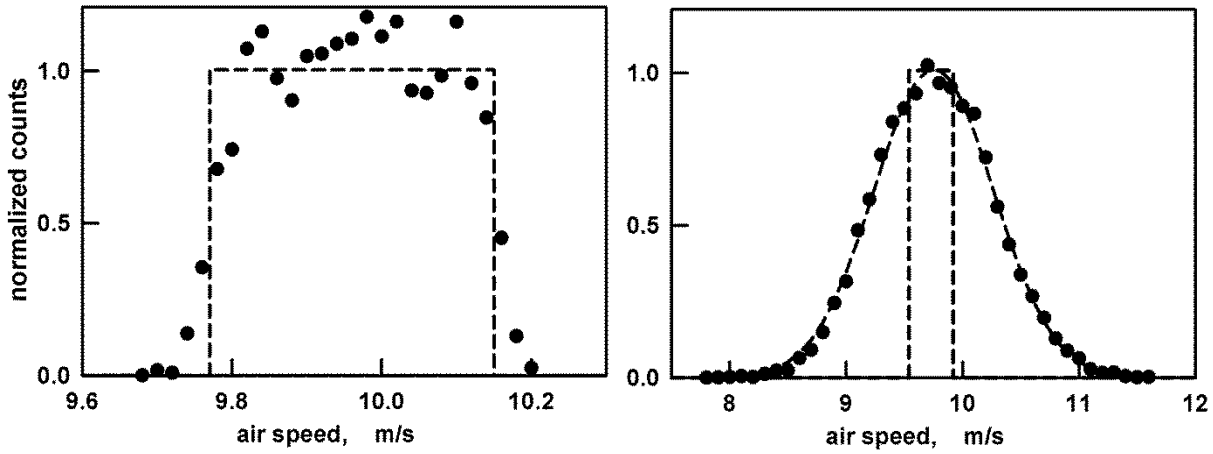

Figure 4. Output from the LDA's burst-spectrum analyzer for two runs with air speeds $\langle V \rangle \approx 9.7$ m/s. LEFT: "zero" turbulence intensity $Tu \approx 0.11$; RIGHT: $Tu = 0.52$ with zero-intensity spectrum shown as dashed rectangle. The smooth curve on the right is a Gaussian function that was fitted to the plotted points.

0.011. The uncertainty of the LDA measurement of *Tu* diverges as *Tu* decreases because Eq. (1) has the subtraction $\sigma^2_{Tu} - \sigma^2_{BG}$. The values of σ_{BG} were greater than zero because the optical interference fringes formed by the LDA in its sensing volume are not exactly parallel, equally-spaced, planes. Because of this spatial dependence of the LDA's sensing volume, a time-independent velocity field generated a rectangular-shaped burst spectrum with half-width of approximately ±0.2 m/s when the average air speed was 10 m/s. This effect introduces large uncertainties when the LDA is used to measure turbulence intensity below 1%. Because the time-dependent and space-dependent contributions to the width of the burst spectrum are uncorrelated, the difference of squared standard deviations in Eq. (1) includes no cross correlation term.

3.2 Measuring turbulence with a high-frequency, 3-D, multi-hole pressure probe

Our second method of measuring the turbulence intensity used a multi-hole pressure probe: TFI Series 100 Cobra Probe manufactured by Turbulent Flow Instrumentation (TFI, Australia)[1]. Often, this probe is used to measure flows surrounding models in wind tunnels because of its small size, frequency response to 2500 Hz, and integrated pressure sensors and electronics. This probe has four holes that can be used to determine the air velocity vector and the static pressure. We determined the turbulence intensity from the output from the manufacturer's electronics package using only the velocity component parallel to mean flow (the X-coordinate) so that the multi-hole results could be compared with the results from the other 1D probes. The most recent designs of multi-hole pressure probes [13, 14] enable turbulence measurements in the range up to 2.5 kHz. Increasing the frequency range was achieved by eliminating tubing connections and placing diferential pressure sensors near the pressure holes.

3.3 Measuring turbulence with a constant-temperature, hot-wire, anemometer

The third instrument that we used to measure turbulence intensity was a Model 54N80 Multi Channel CTA a constant-temperature, hot-wire anemometer manufactured by Dantec[1] Inc. To convert CTA voltage output to air speed, the probe was calibrated against NIST's LDA working standard in the range

from 3 m/s to 27 m/s. We collected hot-wire air-speed data at the rate of 10 kHz using a high speed data acquisition system. [15]

Figure 5 displays four measurements of $PD(V)$, the probability densities that the air-speed V will be measured in a turbulent flow. The plotted values were deduced from measurements that were made at two different distances downstream (80 cm and 220 cm) from the wooden, turbulence-generating grid using two different instruments: a hot-wire anemometer (TA) and the multi-hole pressure probe (M-H P). The probability densities from the multi-hole pressure probe (M-H P) and the hot-wire anemometer (TA) are in mutual agreement. (See Fig. 5.)

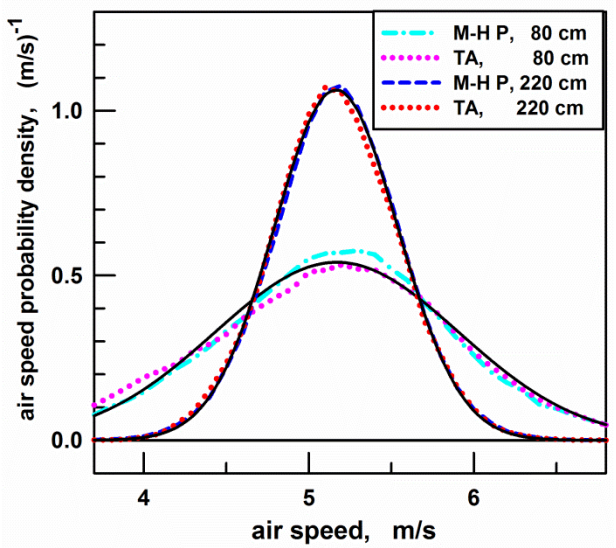

Figure 5. Air-speed probability densities measured with multi-hole pressure probe (M-H P) and hot wire anemometer (TA) at 80 cm and 220 cm downstream from the wooden grid. The black curves are Gaussian functions (Eq. 2) with $\langle V \rangle$ = 5.17 m/s and σ_V = 0.74 m/s at 80 cm and $\langle V \rangle$ = 5.16 m/s and σ_V = 0.37 m/s at 220 cm.

The smooth black curves in Fig. 5 are Gaussian functions with the form

$$PD(V) = \frac{1}{\sigma_V \sqrt{2\pi}} \exp\left[-\frac{1}{2}\left(\frac{V - \langle V \rangle}{\sigma_V} \right)^2 \right] , \qquad (2)$$

that were fitted to the average of the M-H P data and the TA data. For the data 80 cm downstream from the grid, the fitted Gaussian function's parameters were: $\langle V \rangle$ = 5.170 m/s, σ_V = 0.739 m/s, and the corresponding turbulence intensity is Tu = 0.14. At 220 cm downstream, the fitted Gaussian parameters were $\langle V \rangle$ = 5.165 m/s, σ_V = 0.375 m/s, and Tu = 0.073.

3.4 Measuring turbulence with an L-shaped pitot tube

The fourth instrument that we used to measure turbulence intensity was a model 160E-1, L-shaped pitot tube manufactured by Dwyer Instruments Inc[1]. This pitot tube had an insertion length of 0.2 m. Two flexible polymer tubes (5 m long, 6 mm inside diameter) connected the pitot tube to a differential pressure transducer Model 698A manufactured by MKS[1] instruments. The differential pressure transducer had a full scale range of 10 Torr (1 Torr ≈ 133 Pa) and it was connected to an MKS Type 270 signal conditioner that has a 10 V analog output. The averaging time for the signal conditioner was set to the manufacturer's minimum value 4 ms. We computed the turbulence intensity from the standard deviation of the differential pressure Δp data σ_p using the relation $Tu_{\text{L-pitot}} = \sigma_p/(2\langle \Delta p \rangle)$. The lowest panel in Fig. 3 shows that the turbulence intensity deduced from the L-shaped pitot tube was only 19 % to 37 % of the turbulence intensity deduced from the LDA, the hot-wire anemometer, or the multi-hole pressure probe. The horizontal dashed lines in Fig. 3 suggest that these anomalously-low, L-pitot values of the turbulence intensity are approximately independent of the turbulence intensity; however, the low values are a monotonically decreasing function of the air speed. This led us to represent the L-pitot data as the product $f(V) \times g(Tu_{\text{LDA}})$, where $f(V)$ is a function only of the air speed and $g(Tu_{\text{LDA}})$ is a function of the

turbulence, as measured with the LDA. (We would have obtained similar, but noisier results if we had chosen g to be a function of either $Tu_{\text{hot-wire}}$ or $Tu_{\text{multi-hole}}$).

As shown in Fig. 6, the function

$$\frac{Tu_{\text{L-pitot}}}{Tu_{\text{LDA}}} = 0.72\left\langle V\right\rangle_{\text{LDA}}^{-0.42}\left[0.75 + 5.2\,Tu_{\text{LDA}} - 19\,Tu_{\text{LDA}}^2\right] \tag{3}$$

is a satisfactory representation of nearly all the values of the turbulence intensity deduced from the pressure fluctuations measured using the L-shaped pitot tube.

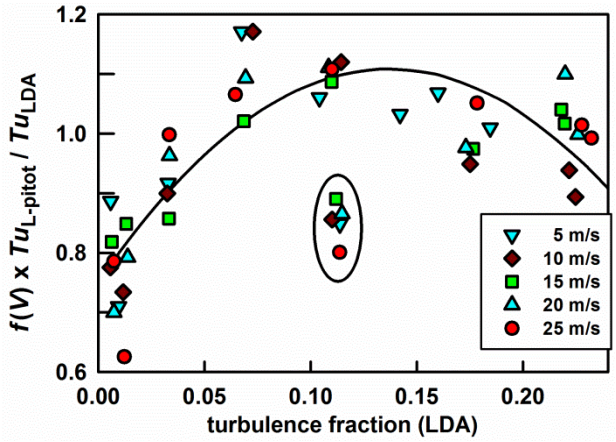

Figure 6. Representation of the L-shaped pitot tube measurements of the turbulence intensity generated by the wood grid. The solid curve is a plot of Eq. (3). The outlying, circled points are discussed in the text.

If it were necessary to use the pressure fluctuation data $Tu_{\text{L-pitot}}$ to determine the turbulence intensity, Eq. (3) could be solved numerically for Tu_{LDA}. However, values of Tu obtained in this way would not be trustworthy unless the L-shaped pitot tube was used in exactly the same configuration that was used to determine Eq. (3). We emphasize that "exactly the same configuration" implies using the same differential pressure transducer and the same tubes connecting the pressure transducer to the pitot tube.

In Figure 6, the circled, exceptional values were obtained when the L-shaped pitot tube was 70 cm downstream from the wooden turbulence-generating grid. We speculate that, at 70 cm, the turbulence intensity retained some of spatial structure generated by the 15 cm pitch of the grid. The other data in Fig. 6 were measured 130 cm downstream from the grid.

4. Turbulence-dependent calibrations

In Sect. 3, and especially in Figs. 3 and 5, we established that turbulence intensities generated in NIST's wind tunnel can be reliably measured with either an LDA, multi-hole pressure probe, or hot-wire anemometer. Therefore, NIST is now able to calibrate anemometers as a function of turbulence intensity, as well as a function of air-speed, pitch angle, and yaw angle. We demonstrate this new capability with exploratory measurements using an L-shaped pitot tube, an S-probe, and a 5-hole pressure probe.

4.1 Calibrating an L-shaped pitot tube.

Figure 7 displays the turbulence-dependence of the calibration factor CF of an L-shape pitot tube.

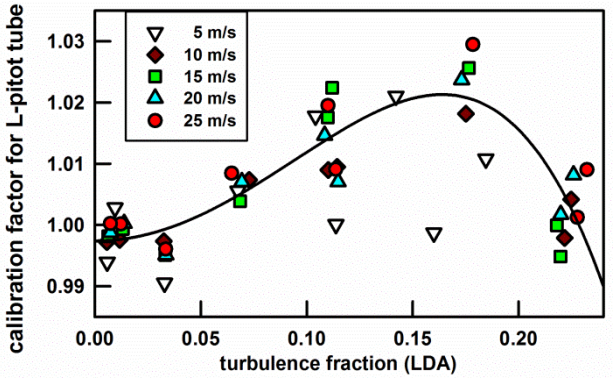

Figure 7. Turbulence intensity dependence of the calibration factor of L-shaped pitot tube.

The smooth curve represents the data at 10 m/s, 15 m/s, 20 m/s, and 25 m/s using the function:

$$CF = 0.997 + 1.78\,(Tu)^2 - 33\,(Tu)^4 \qquad (4)$$

Bradshaw and Goodman [16] reviewed a wide range of conditions that lead to the prediction $CF = 1 + a_2(Tu)^2$ with $a_2 > 0$, as in Eq. (4). However, we are not aware that a term of the form $a_4(Tu)^4$ has been predicted.

In Fig. 7, our preliminary data at 5 m/s are more widely scattered than the data at higher air speeds. For these data, these average values of the calibration factor are somewhat smaller than the empirical function, Eq. (4).

In summary, the calibration function for the particular L-shaped pitot tube that we studied varies by approximately 2 % for air speeds in the range 5 m/s to 25 m/s and for turbulence intensities in the range of 0 % to 23 % .

4.2 Calibrating an S-type probe

Figure 8 contains two photographs of an S-type pitot tube (S-probe) manufactured by Apex Instruments.[1] As indicated in Fig. 8, an S-probe has two pressure-sensing ports that face in opposite directions. Each port is connected to a tube that leads to a differential pressure gauge that measures the pressure difference between the ports $\Delta p_{\text{S-probe}}$. S-probes are called two-dimensional (2-D) probes because they are used to measure one angle (yaw) and one flow-velocity component (the component along an imaginary line connecting the centers of the pressure ports).

S-probes are widely used to conduct relative accuracy tests of the continuous emission monitoring systems (CEMS) that are installed in the flue-gas stacks of coal-burning power plants. The CEMS monitors the performance of the power plant's pollution control systems, as mandated by the US Environmental Protection Agency. When S-probes are used to audit CEMS, they are moved in steps ("traversed") along horizontal diameters through the flue-gas stack to map a horizontal cross section of the stack's flow field $V(r)$ at discrete points. (Here, r is a coordinate that measures the distance from the center of the stack.) Then, $V(r)$ is integrated to determine the flue-gas flux. The flue-gas flux is combined with flue-gas composition measurements to determine the quantity of pollutants emitted by the stack. Recently, the Environment Protection Agency (EPA) declared that carbon dioxide (CO_2) is a pollutant that must

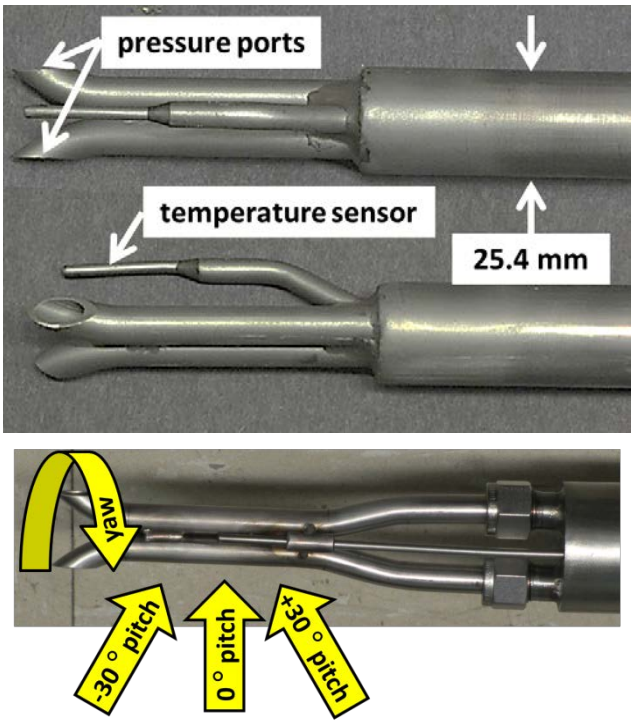

Figure 8. Top: Two photographs of the S-probe that we calibrated. Bottom: Another S-probe showing the definitions of pitch and yaw angles.

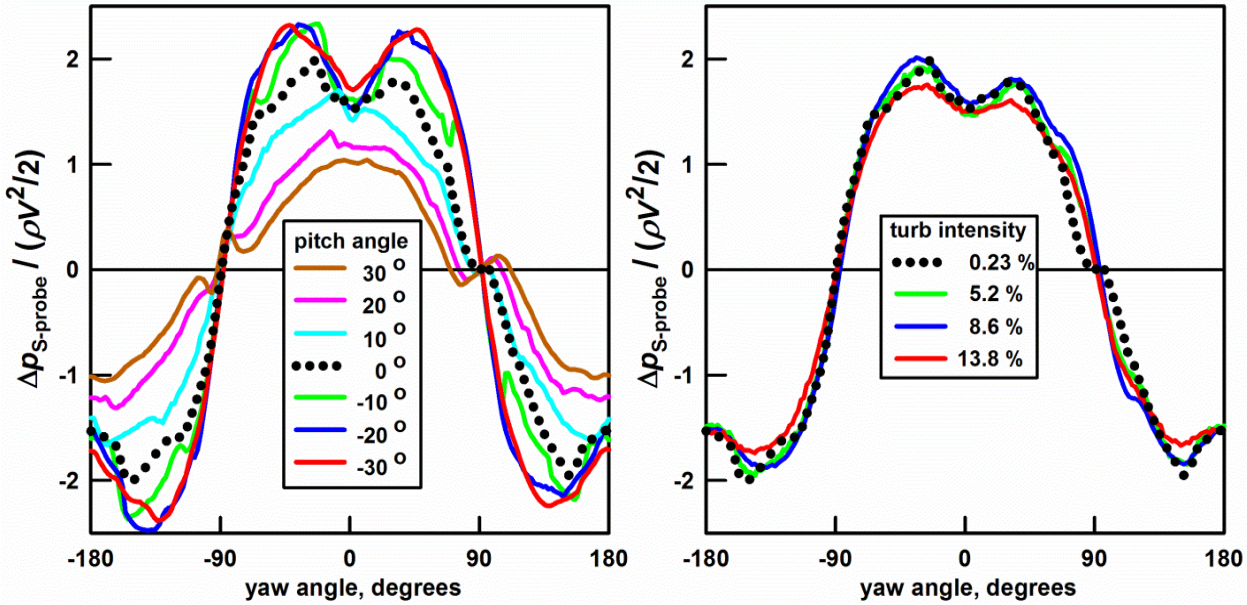

Figure 9. Calibration of an S-probe as a function of yaw angle. LEFT: Pitch angle varies from –30 ° to 30 ° with 0.23 % turbulence intensity. RIGHT: Turbulence intensity varies from 0.23 % to 13.8 % with 0 ° pitch.

be regulated. If a price is put on CO_2 emissions, the need will arise to reduce the uncertainty of the measurements of the flue-gas flux using S-probes.

When S-probes are used to map $V(r)$, the S-probe is rotated about its long (yaw) axis (horizontal in Fig. 8) at each discrete measurement point until the pressure difference between its two ports is zero. In that configuration, the faces of the probe's ports are parallel to the flow and an imaginary line connecting the centers of the faces is perpendicular to the flow. The rotation angle measured from the ports' vertical orientation is the yaw angle between the S-probe and the gas flow at the measurement point. Then, at the same measurement point, the S-probe is rotated –90 ° in yaw and the differential pressure $\Delta p_{\text{S-probe}}$ is measured. This pressure difference is used to determine the flow velocity at the measurement point. Note: this procedure does not account for the pitch angle, which is the angle between the long axis of the S-probe and the component of the flow velocity measured by the S-probe. (See Fig. 8, bottom.) However, the calibration of S-probes is sensitive to the pitch angle. (Fig. 9, left) Therefore, S-probe measurements of flue-gas flux will have errors if the flow has a significant radial component.

Figure 9 displays a fraction of the extensive S-probe calibration data obtained in NIST's wind tunnel. The quantity plotted is the pressure calibration coefficient which we define as the ratio of the measured differential pressure $\Delta p_{\text{S-probe}}$ to the dynamic pressure $\rho V^2/2$, where ρ and V are the mass density and the mean speed of the air in the wind tunnel, respectively. For measuring flue-gas flows, the important parts of these calibration data occur near yaw angles of +90 ° where $\Delta p_{\text{S-probe}}$ vanishes and near yaw angles of 0 °, where the measured value of $\Delta p_{\text{S-probe}}$ is used to compute the axial component of the air velocity vector.

The left panel of Fig. 9 shows that near 0 ° yaw, $\Delta p_{\text{S-probe}}/(\rho V^2/2)$ varies by approximately 13 % for pitch angles in the limited range 0 ° ± 10 °. In contrast, the right panel of Fig. 9 shows that near 0 ° yaw, $\Delta p_{\text{S-probe}}/(\rho V^2/2)$ varies by only 3 % for turbulence intensities ranging from 0.23 % to 13.8 %. In NIST's

wind tunnel, the lowest turbulence intensity is 0.23 %. (To date, NIST calibrates air speed sensors in this low turbulence.) The highest turbulence intensity 13.8 % is comparable with the 12% turbulence intensity [17] that has been found in some flue-gas stacks.

We generalize Fig. 9 by asserting that the S-probe's sensitivity to pitch angles leads to greater measurement uncertainties than the S-probe's sensitivity to turbulence intensity. This is confirmed by extensive NIST calibrations (not shown) conducted with both non-zero pitch and significant turbulence intensity.

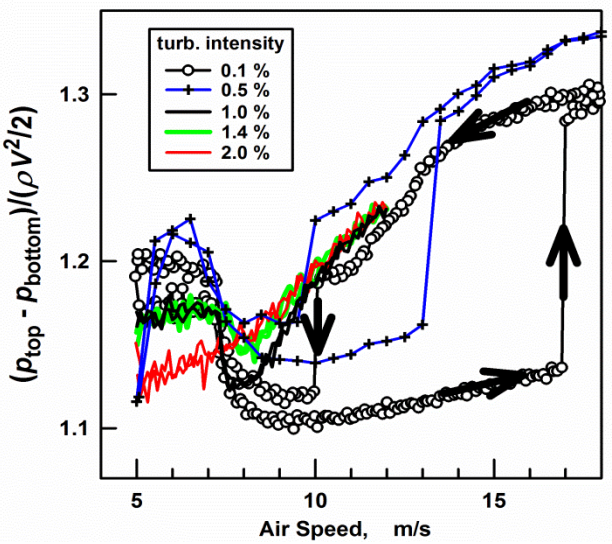

Figure 10. Scaled pressure differences from Ref. [4] for a 5-hole pressure probe at 20 ° yaw. The arrows on the data for the turbulence intensity *Tu* = 0.1 % show that the lower branch of the hysteresis loop was measured while the air speed increased from 5 m/s to 18 m/s and the upper branch was measured while the air speed decreased. Hysteresis is absent when *Tu* ≥ 1 %.

4.3 Calibrating a 5-hole pressure probe.

Recently, Crowley *et al*. [4] used NIST's wind tunnel to calibrate a cone-shaped, five-hole, pressure probe model DC-250-78.72-J-76.72-CD manufactured by United Sensor Corp.[1] When this pressure probe was oriented 20 ° ± 5 ° in yaw and 0 ° in pitch with respect to the wind tunnel's axis, Crowley *et al*. discovered hysteresis in the differences of the pressures ($p_{top} - p_{bottom}$) measured between the hole on the top of the probe and the hole on the bottom of the probe. In Fig. 10, we re-plotted the data from Crowley *et al*.'s Fig. 4. [The plotted values of ($p_{top} - p_{bottom}$) are scaled by the dynamic pressure, $\rho V^2/2$,] As indicated by the arrows in Fig. 10, the values of ($p_{top} - p_{bottom}$) measured while the air speed increased from 5 m/s to 18 m/s were up to 30 % larger than ($p_{top} - p_{bottom}$) measured while the air speed decreased. This hysteresis during the calibration of pressure probes is not well-known in the literature of air speed measurements; however, similar hysteresis is well-known in the literature of airfoils where it is associated with stall. [18]

In Fig. 10, the largest hysteresis occurred at the lowest turbulence intensity, Tu = 0.001. The hysteresis decreased with increasing turbulence; hysteresis was not detected when $Tu \geq 0.01$. These data dramatically illustrate the idea that a calibration of this five-hole pressure probe in a low-turbulence wind tunnel would be irrelevant if the probe were used to measure flows with $Tu > 0.01$.

Crowley *et al*. [4] showed that the hysteresis was associated with flow separation and recirculation near the top hole used to measure ($p_{top} - p_{bottom}$). Because flow separation and recirculation are common phenomena; the hysteresis displayed in Fig. 10 is likely to occur during the calibration of other multi-hole pressure probes and probably at other pitch and yaw angles.

5. Summary

We designed and manufactured a 3-D calibration rig to calibrate 3-D airspeed probes. We installed a set of turbulence generators that generate turbulence intensities spanning the range 0.1 % < *Tu* < 20 %. We showed that the turbulence intensity is an additional variable which is sometimes important for making accurate calibrations. We tested 4 pressure probes: L-shaped pitot tube, a 4-hole ("Cobra") pressure probe, an S-type probe, and a conical, 5-hole pressure probe. For the widely used L-shaped and S-probe, we measured 2 % to 3 % effects on calibration factor. At low turbulence levels, the pressure calibration factor of our 5-hole pitot tube had up to 20 % hysteresis in specific airspeed and angle ranges. This effect is associated with flow separation; therefore, we expect it to occur with many multi-hole pressure probes. The hysteresis gradually disappears with increasing turbulence intensity.

Acknowledgements

We thank Gregory Scace for his help in designing and manufacturing 3-D calibration rig. We thank Chris Crowley, Joey Boyd, and James Filla for their contributions to the early stages of this research and we thank Rodney Bryant for his careful reading of this manuscript.

References

[1] Yeh, T. T., Hall, J. M., *Air Speed Calibration Servic.* NIST Special Publication 250-79, National Institute of Standards and Technology, Gaithersburg, Maryland, 2006.

[2] Jewel B. Barlow, William H. Ray, Alan Pope. *Low-Speed Wind Tunnel Testing*, 3rd Edition, 1999, ISBN: 978-0-471-55774-6

[3] Jorge Colman Lerner (Editor). *Air Speed Measurement Standards Using Wind Tunnels, Wind Tunnels and Experimental Fluid Dynamics Research, Chapter 9 Air Speed Measurement Standards Using Wind Tunnels* written by Sejong ChunInTech. ISBN: 978-953-307-623-2

[4] Christopher Crowley, Iosif I. Shinder, Michael R. Moldover. *The effect of turbulence on a multi-hole Pitot Calibration*, Flow Measurement and Instrumentation Vol. 33, October 2013, pp. 106-109, ISSN 0955-5986.

[5] L. F. G. Simmons and C. Salter. *Experimental Investigation and Analysis of the Velocity Variations in Turbulent flow*, Proc Roy Soc London A, Mathematical and Physical Sciences, Vol. 145, pp. 212-234 (1934)

[6] G. I. Taylor. *Statistical Theory of Turbulence II*, Proceeding of the Royal Society of London. Series A. Mathematical and Physical Sciences, Vol. 151, No. 873, pp. 444-454.

[7] Hyung Suk Kang, Stuart Chester, Charles Meneveau. *Decaying turbulence in an active-grid-generated flow and comparisons with large-eddy simulation*, J. Fluid Mech. 2003, Vol. 480, pp. 129–160.

[8] Thomas Kurian and Jens H M Fransson. *Grid-generated turbulence revisited*, Fluid Dyn. Res. Vol. 41, 2009.

[9] Jon V. Larssen, William J. Devenport. *On the Generation of Large-Scale Homogeneous turbulence*, Exp. Fluids 2011 Vol. 50, pp. 1207–1223.

[10] Emmanuel Virota, Xavier Amandolesea, Pascal Hémona. *Unsteady forces induced by a flag in a wind tunnel*,2013, 21ème Congrès Français de Mécanique Bordeaux, 26 au 30 août.

[11] Sébastien Michelin, Stefan G. Llewellyn Smith, and Beverley J. Glover. *Vortex shedding model of a flapping flag*, J. Fluid Mech 2008, Vol. 617, pp. 1-10.

[12] Jon Vegard Larssen. *Large Scale Homogeneous Turbulence and Interactions with a Flat-Plate Cascade*, Ph.D. thesis, Virginia Polytechnic Institute, January 25th, 2005, Blacksburg, Virginia.

[13] Watkins, S., Mousley, P. & Vino, G. *The development and use of dynamic pressure probes with Extended Cones of Acceptance (ECA)*, Proceedings of the 15th Australasian Fluid Mechanics Conference, 13-17 December, 2004, Sydney, Australia.

[14] Demetri Telionis, Yihong Yang. *Recent Developments in Multi-Hole Probe (MHP) Technology*. 20th International Congress of Mechanical Engineering November 15-20, 2009, Gramado, RS, Brazil

[15] Shinder, I. I., Crowley, C. J., Filla, C. J. and Moldover, M. R. *Improvements to NIST's Air Speed Calibration Service*, Flow Measurement and Instrumentation, In Press, Corrected Proof Available online December 8 2014

[16] P. Bradshaw and D. G. Goodman. *The Effect of Turbulence on Static-Pressure Tubes*, Aeronautical Research Reports and Memoranda, R. & M. No. 3527, Her Majesty's Stationary Office, London, 1966.

[17] Steffan Johnson, US EPA, private communication, May 2014.

[18] Z. Yang, H. Igarashi, M. Martin, H. Hu. *An Experimental Investigation on Aerodynamic Hysteresis of a Low-Reynolds Number Airfoil*. 46th AiAA Aerospace Science Meeting and Exhibit 2008, Reno, Nevada.